Satellite Interferometry as a Tool for Early Warning and Aiding Decision Making in an Open-Pit Mine

Emanuele Intrieri, Tommaso Carlà, Paolo Farina, Federica Bardi, Hakki Ketizmen, and Nicola Casagli

***Abstract*—Slope failures are life-threatening geohazards well-known in the mining industry, where a single accident can endanger workers and cause million dollars' -worth of activity downtime. Therefore, a detailed ground deformation map of an open-pit mine represents a vital planning tool and high-frequency monitoring is pivotal, since false or anticipated alarms may represent a higher impact than missed alarms. This article presents an application of interferometric satellite data from Sentinel-1. The scope of the study is showing the potential of the new generation of satellites for the detection of the boundary, typology, and kinematics of the on-going slope instabilities in open-pit mines. Most notably, this experience discloses how the short revisiting time (six days) permits the implementation of time of failure forecasting methods, which so far were a prerogative of ground-based monitoring systems. Only recently, a few experiences have shown the possibility of (*a posteriori*) predicting slope failures using displacement time series measured from satellite; the case study here described represents one of such first examples. Moreover, 11 other areas of instability have been detected and classified in terms of subsidence (sediment compaction) or slope failures, based on considerations concerning the acquisition geometry used to detect the movements. The movement vectors along the ascending and descending lines of sight have been combined to compute horizontal and vertical vectors, which have been employed to infer the geometry of the sliding surface of some selected slope instabilities. Despite the advancements of the technique, clear limitations still exist and are discussed in this article.**

***Index Terms*—Earth observation, landslide hazard, mapping, monitoring¸ remote sensing.**

I. Introduction

THE MANAGEMENT of unstable slope is a fundamental challenge in open-pit mines, mainly aimed at maintaining the safety of mine operations and at reducing perspective economic losses. In this context, an adequate early warning system is a valuable tool to reduce the impact of slope failures on the mine life.

An early warning system is mainly made by following four components:

1) design;
2) monitoring;
3) forecasting;
4) education [1].

Among them, monitoring and forecasting activities represent operational steps, and their efficiency is strongly related to the performance of the techniques employed in the monitoring phase, which influences the goodness of the acquired data and consequently the forecasting results.

Common instruments deployed for safety critical monitoring in open-pit mines are extensometers [2], total stations, and GNSS receivers [2]–[4]. Lately, after 20 years of experimentations in different fields [5]–[8], ground-based interferometric synthetic aperture radar (GB-InSAR), or slope stability radar as it is most known in the mining industry, stood out as the cutting-edge technology for real-time slope failure monitoring aimed at identifying critical displacement thresholds useful for triggering response plans in open-pit mines [9], [10].

Also satellite InSAR techniques are employed in monitoring slope stability [11]–[17], as well as other natural phenomena that induce terrain deformation, such as earthquakes [18], [19], volcanic activity [20]–[22], ground subsidence and uplift [23]–[27], glacier motion [28]. Traditionally, satellite InSAR techniques are mostly used for long-term monitoring, ground deformation mapping, and landslide inventories [29], [30], whereas early warning applications were out of reach, due to limitations in the data acquisition frequency, until recently [31]. During the last 25 years, satellite techniques have seen an increasingly greater diffusion. Thanks to their inherent characteristics, they present several of advantages in the field of monitoring activities, such as they are able to observe the investigated scenario in any lighting and weather condition, producing displacement maps at a large scale, with millimetric accuracy and without physical access to the observed area [32].

Among the other characteristics, the sensor revisiting time (the time elapsed between two consecutive interferometric observations of the same area by a sensor) plays a key role in the satellite capability to detect deformation phenomena over time. The revising time, together with the synthetic aperture radar (SAR) wavelength, influences the detectable velocity of the deformation phenomena, which is limited by the ambiguous nature of the interferometric products [32]. In this sense, the ESA Sentinel mission represents a step forward in the field of satellite SAR sensors; the mission is made by a constellation of

Manuscript received December 4, 2018; revised May 3, 2019, July 15, 2019, and September 19, 2019; accepted November 8, 2019. Date of publication December 22, 2019; date of current version February 4, 2020. *(Corresponding author: Emanuele Intrieri.)*

E. Intrieri, T. Carlà, F. Bardi, and N. Casagli are with the Department of Earth Sciences, Università degli Studi di Firenze, Firenze 50121, Italy (e-mail: emanuele.intrieri@unifi.it; tommaso.carla@unifi.it; federica.bardi@unifi.it; nicola.casagli@unifi.it).

P. Farina is with the Geoapp s.r.l., Academic Spin Off of the Università degli Studi di Firenze, Firenze 50125, Italy (e-mail: paolo.farina@geoapp.it).

H. Ketizmen is with the Ciner Group, Sim Söğütözü İş Merkezi, Ankara 06560, Turkey (e-mail: h.ketizmen@cinergroup.com.tr).

This article has supplementary downloadable material available at http://ieeexplore.ieee.org, provided by the authors.

Color versions of one or more of the figures in this article are available online at http://ieeexplore.ieee.org.

Digital Object Identifier 10.1109/JSTARS.2019.2953339

two satellites, Sentinel-1A and Sentinel-1B, launched in April 2014 and April 2016, respectively. They are able to provide large-scale mapping (250 km swath and 165 km azimuth width) with short revisiting times (down to six days) and are equipped with a C-band sensor [33]–[35].

Under theoretical conditions, without noise and applying adequate algorithms of phase unwrapping to solve the problem of phase ambiguity, Sentinel sensors are able to detect velocity values up to 42.6 cm/year [32].

The main objective of this research has been the exploitation of satellite interferometric data belonging to the Sentinel constellation, to support the investigations related to unstable slopes in a copper open-pit mine in an undisclosed location. The use of such data was not only limited to the identification of unstable areas, but also permitted to identify time series indicating a forthcoming failure and theoretically allowing for a slope failure forecasting or, at least, an aware planning and business continuity management (BCM) [2].

Displacement time series represent one of the products of satellite SAR interferometry, providing the deformation history over the observed datasets. The reduced revisiting time of the Sentinel constellation enables to derive detailed information from deformation time series; specifically, here an attempt is presented to apply the inverse velocity method [36] on satellite SAR time series to provide the time of failure of an unstable slope, in an open-pit mine. Such applications are still pioneering; since a real forecasting (i.e., not made *a posteriori*) has not been documented yet, every experience that can prove its feasibility assumes a great importance [37]–[39].

The short revisiting time of the Sentinel data, together with the availability of SAR historical datasets, is an important tool to analyze not only displacement maps, but also displacement time series, allowing the operators to clearly delimitate the unstable areas and to make predictions on the time of failure with adequate advance warning.

A limitation to the applicability of the InSAR techniques described here is that they typically require large sets of multitemporal data for the processing, which, in some cases, may be conflicting with the need for fast responses in the framework of an early warning system.

II. Materials and Methods

A. InSAR Technique

Satellite SAR sensors are side-looking radar and operate with a LOS direction tilted with respect to the vertical direction. Because of the incidence angle (usually ranging between 23° and 45°), the sensor is much more sensitive to vertical deformation than to horizontal deformation.

The satellites orbit the Earth following sun-synchronous, near-polar paths, with an altitude ranging between 500 and 800 km above the surface. Combining the Earth's rotation movement with their orbits, satellites are able to gather information about the same target with two opposite acquisition geometries: ascending (from the South Pole to the North Pole) and descending (from the North Pole toward the South Pole). These radar signals are transmitted in pulses by a microwave beam, illuminating a swath. Each backscattered pulse is recorded by the receiver, and then it is processed to produce a spatial image from raw SAR signals.

Starting from SEASAT, the first satellite with an imaging SAR, several international SAR missions have been launched in the past and several are still active; an exhaustive review of the satellite SAR sensors, their main characteristics, and acquisition times are reported in [40].

Spaceborne SAR instruments usually operate either at X-, C-, or L-band of the microwave portion of the electromagnetic spectrum, covering areas up to 100 square kilometers, with a resolution of a few meters.

Space-borne InSAR is an effective technique for ground deformation measurements over large areas, ideal for monitoring subvertical displacements of the ground surface. It is an active remote sensing technique: The sensors emit a microwave radiation in order to scan objects and areas, recording the backscattering radiation of the target.

One of the most common applications of these data makes use of the InSAR technique, which consists in comparing the phase matrixes of two SAR images, acquired in different times from the same point, making it possible to estimate the displacement of the observed area, by analyzing the related phase displacement of the reflected waves. The result is an image called "interferogram," that includes the phase displacement occurred in the time interval between two subsequent acquisitions [41]–[46].

Depending on the specific processing convention adopted, it is possible to uniquely define the phase only within a certain range (e.g., between $-\pi$ and π) and any value outside this interval is "wrapped." We cannot solve the ambiguity due to the impossibility of distinguishing between phases that differ by 2π [47].

The classical approach to retrieve displacement information from satellite radar data is the differential InSAR technique, which reveals some limitations, mainly related to temporal and geometrical decorrelation and atmospheric noises [32], [48]. These limitations have been partially overcome by the development of multitemporal interferometric approaches, such as permanent scatterer (PS)-InSAR and SqueeSAR [49], that imply a reduction of the atmospheric impact on the estimated displacement values by using long temporal series of SAR images.

PS are single radar targets (typically roads, buildings, and other urban elements) that are able to maintain a stable scattering behavior, high coherence values, and high electromagnetic reflectivity. These features enable to easily correct the topographic and noise contribution to the interferometric phase, whereas the atmospheric term can be removed: In fact, through a statistical analysis of the signals backscattered from highly coherent targets, this approach retrieves estimates of the displacements occurring between different acquisitions by distinguishing the phase shift related to ground motions from the phase component due to atmosphere, topography, and noise [25], [49].

One of the limitations of this technique is that, for their characteristics, PS are scarcely present in nonurban areas. The SqueeSAR technique partially reduces this restriction by analyzing, beside PS, also the so-called distributed scatterers (DS), which are represented by homogeneous areas spread over a group of pixels in a SAR image (fields, bare soil, shrubs). In this way, the density of measurements points, especially in rural areas, is significantly increased [50]–[52].

More in detail, DS are identified through the following steps:

1) selection and analysis of image pixels;
2) statistical comparison of each pixel with the adjacent ones;
3) further processing and analysis of statistically homogenous pixels;
4) identification of DS within statistically homogeneous areas.

Once defined, DS are processed using the PSInSAR algorithm and provide the same kind of information, in the form of deformation maps and displacement time series of each measurement point. The same considerations concerning atmospheric noise are applied.

In the copper open-pit mine presented here, given the small extent of the area, the impact of the atmospheric noise was not relevant, except for those points that, in winter season, were particularly noisy due to the presence of snow and that have been consequently removed.

The interferometric measurements are relative to a reference point and a reference date, (i.e., the first date available). The criteria used to select the reference point are as following.

1) It must be in a stable zone, also considering any prior information about land motion (e.g., previous InSAR data and GNSS) and, in the case presented here, taken from outside the extracting area.
2) In a possibly central position to minimize the impact of any spurious signal dependent on the distance from the reference point.
3) It must display a high coherence (i.e., high value and low dispersion of the amplitude time series).

B. Slip Surface Calculation

In order to support the interpretation of the deformations detected by satellite InSAR, a method was implemented, which was theorized by Carter and Bentley [53] and further developed by Cruden [54] and is aimed at estimating the depth and geometry of the sliding surface of a slope failure from superficial displacement vectors. This requires the vertical and horizontal components of the movement vector characterizing the radar targets falling within the landslide areas.

Under the assumption of the absence of N–S deformation components, combining ascending and descending information allows one to extract the vertical and horizontal (in the E–W direction) components of the movement and, consequently, the actual vector of displacement [55], [56] (Fig. 1).

To combine ascending and descending datasets and extract the vertical and E-W components of a specific point on the ground, it is necessary to identify a radar target acting as a good scatterer in both acquisition geometries. Practically, identification of the same radar target in both the datasets is often a challenge. Typical values of positioning precision are 7 and 2 m for the E–W and N–S directions, respectively, for radar targets less than 1 km from the reference point and considering a five-year-long dataset of C-band radar images, while precision on elevation values is 1.5 m. Due to this low spatial resolution and to the poor georeferencing accuracy, it is often difficult not only to identify exactly what object is acting as the "persistent scatterer" but, provided that the scattering object is identified, also to detect which part of the object is actually scattering and, furthermore, to be able to see it in both orbits.

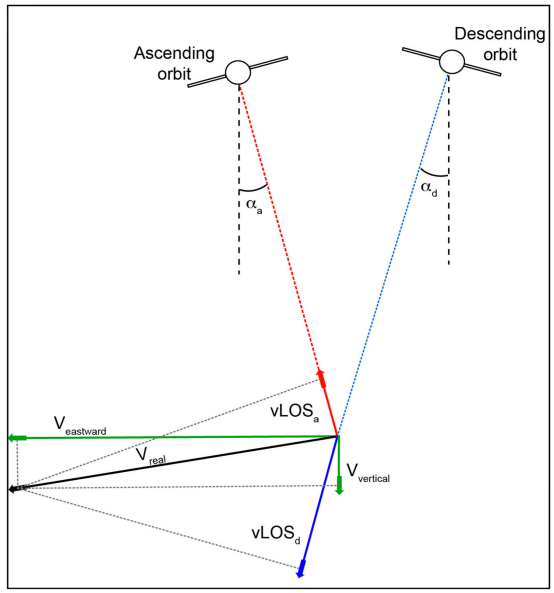

Fig. 1. Graphical scheme of the decomposition of a vector according to the geometry of each orbit and the horizontal (eastward) and vertical directions. Modified from [57] and [58].

To overcome this limitation, the datasets of radar target points have been resampled by means of a regular grid, characterized by a predefined spacing interval. For each grid cell and for both the ascending and descending geometries, the mean value of the velocities of the radar targets contained within the cell is then calculated. In general, interpolation artefacts due to this resampling are possible. If the cells are not too large, we can assume that the measuring points within them are similar and referred to the same movement; on the other hand, the averaging process reduces the noise and makes the final value representative of the ongoing deformation for that cell. Hence, a synthetic radar target is generated, with associated ascending and descending velocity estimates. A detailed description and dissertation of this whole approach can be found in [58].

Using the synthetic values and taking into account the orientation of the satellite LOS, the vertical and E–W ground velocity components of movement were then estimated geometrically over the study area. The E–W component was reprojected along the hypothesized planimetric direction of movement of the analyzed instability and successively combined with the vertical component to obtain a vector for each node of the grid. The vectors that were nearest to the topographical cross-section were then used and considered on the cross-section itself (the arrows in Fig. 2). These measurements of superficial ground motion have then been used to estimate the possible geometry of the sliding surface.

In particular, Cruden [54] invented a graphical method (see Fig. 2) that starts with drawing the normals (N_1 and N_2 in Fig. 2) to the first two vectors (the arrows on the left in Fig. 2). The intersection of the two consecutive normals (O_1) is obtained. Centered on O_1, an arc can be drawn starting from the application point of the first vector (that is from the position of the vector on the cross section). The circle is drawn until it reaches the intersection V_1 between the arc and the projection of the normal N_2 to the next vector. V_1 represents the first estimated point

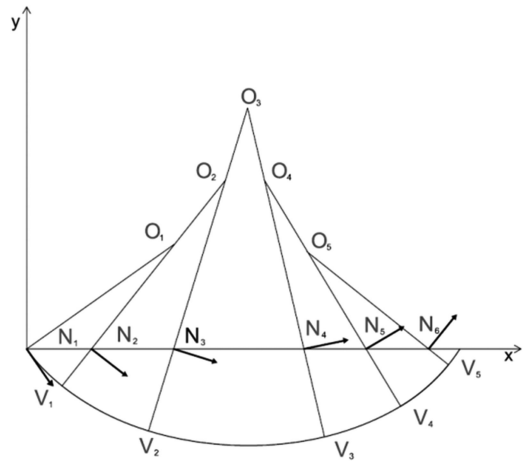

Fig. 2. Calculation of the sliding surface according to the graphical method proposed by Cruden [54], based on Carter and Bentley [53].

of the slip surface. The same procedure is repeated drawing the normal N_3 to the third vector and determining O_2 (see the supplementary material for a step-by-step animation of the entire process shown in Fig. 2).

III. Dataset

A multi-interferogram analysis of the C-band (5.5-cm wavelength) SAR images acquired by the Sentinel satellite constellation from March 2, 2016 to November 21, 2016 have been carried out, in both ascending (satellite track n.145) and descending (satellite track n.50) geometries (see Fig. 3).

The quality of data was good except for some images acquired in wintertime that have been discarded due to the presence of the snow. After this selection, a total of 47 and 49 scenes have been used in descending and ascending geometries, respectively, and been processed in full resolution.

A digital elevation model with a 2 m $\times$ 2 m cell-size resolution has also been used.

Due to the steepness and of the central pit of the mine, the slope exposed toward ESE shows a reduced density of measurement points (PS and DS) that can be obtained from the SAR images, especially for the acquisitions along the descending orbit, as visible in Fig. 3.

The satellite in the ascending orbit moves from SSE to NNW, whereas the one on the descending orbit from NNE to SSW. Both are right-side looking radar, which means that LOS measurements in ascending geometry are characterized by an azimuth of 81.69° (and a vertical angle of 39.22°), whereas LOS measurements in descending geometry feature an azimuth of 282.24° (and a vertical angle of 35.54°). This means that measurements in ascending geometry are slightly more sensitive to ENE–WSW movements, whereas in the case of descending geometry measurements are slightly more sensitive to ESE–WNW movements. In particular, since the movements are considered positive when they move toward the sensor, a westward-moving target will be negative in the descending geometry and positive in the ascending geometry [see the red and blue targets in the central area in Fig. 3(a) and (b), respectively]. Conversely, mainly vertical movements will have the same sign [see the red targets in the bottom part in Fig. 3(a) and (b)].

The sensitivity to the vertical component of ground deformation, although similar, is higher for the descending geometry. As a result, satellite data mostly provide reliable information concerning E–W and vertical movements, whereas limited insight may be gained for predominantly N–S movements. This is a well-known intrinsic limitation of the interferometric technique that might cause to underestimate the risk existing in certain areas. However, it should be noted that slope instabilities can still be detected due to their vertical component. Nonetheless, in general, the integration with other techniques to monitor N–S movements is recommended, whenever possible. In this particular case study, the highest degree of uncertainty related to N–S sensitivity is related to the unstable areas N of the pit (see Figs. 3 and 4), whereas all the remaining slope instabilities have expected directions of movements that are favorably aligned along the satellite LOS.

Available data have been processed by TeleRilevamento Europa company, applying SqueeSAR algorithms [59].

The use of the SqueeSAR algorithms has only been used to increase the number of measuring points, but it is not necessary for the scope of this article, that is to show how Sentinel-1 has been used as an early warning and decision-making tool for the open-pit mine.

IV. Data Interpretation and Discussions

A. Definition of the Unstable Areas

The definition of the boundaries of instability phenomena, mainly slope failures and subsidence areas, is one of the most effective applications of satellite interferometry [40], [60]–[62].

In this case, displacement data were analyzed based on their absolute values, their trends, their acquisition geometry and spatial continuity, coupled with considerations deriving from the analysis of the local morphology and the expected direction of movement in case of slope instabilities. This enabled the delimitation of the main areas of ground deformation within and in proximity of the pit (see Fig. 4).

Where displacements were null, very local, or attributable to noise (e.g., time series displaying very scattered values with no trend) the area was considered stable; where a linear trend was observed, this was considered as an indication of an instability taking place at constant velocity. The highest attention was paid to the recognition of intense accelerations that may be signals of instabilities possibly leading to failure. This behavior, called accelerating creep [63], is typical of the prefailure stage called tertiary creep and is characterized by a hyperbolic increase in the acceleration.

This feature has been first harnessed by Saito [64] who used it to develop an empirical landslide forecasting method, from which a series of graphical solutions [36], [65], [66], methodologies and approaches [67]–[70] were then developed. The most popular method derived from the creep theory is the so-called inverse velocity method [36], [71], [72], according to which it is possible to extrapolate the time of failure of a landslide as the intersection between the inverse of the velocity (v^{-1}) and the time axis, under the hypothesis that as the velocity increases and theoretically tends toward infinite at the time of collapse,

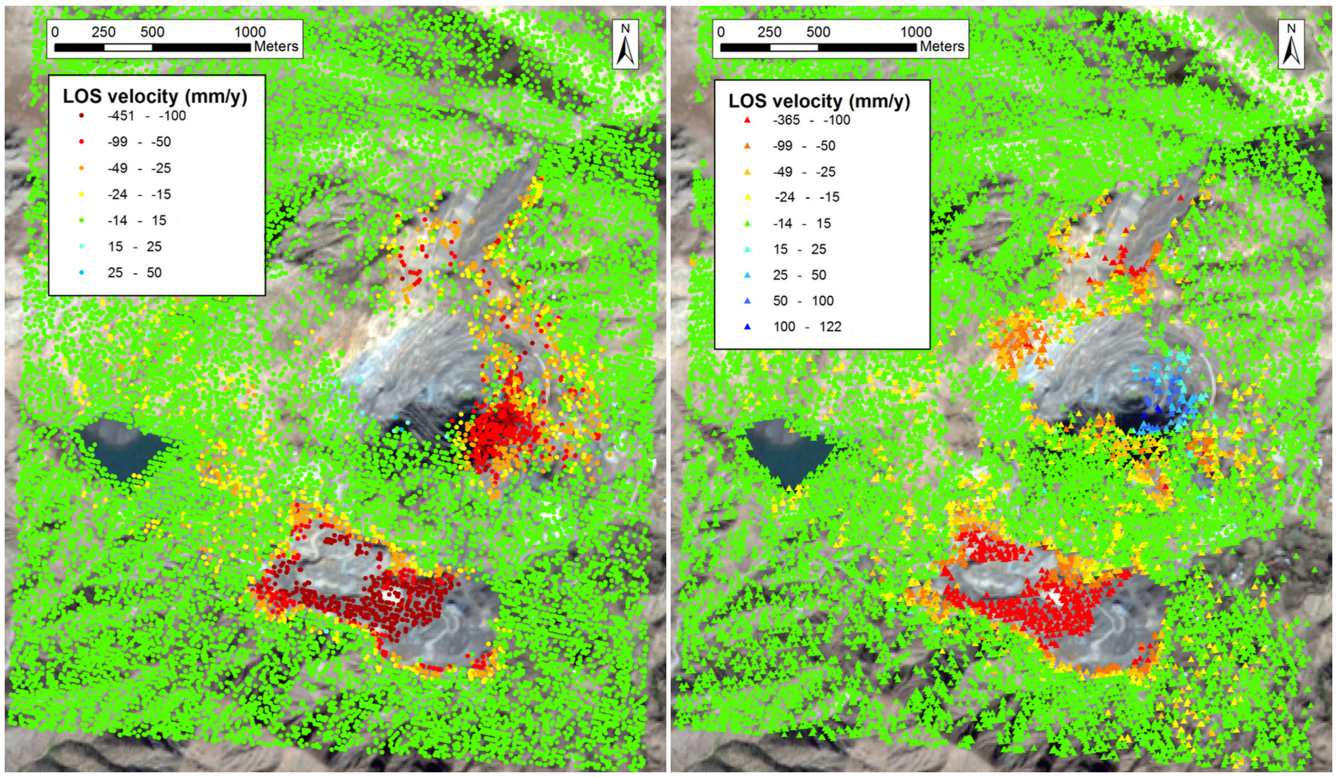

Fig. 3. Satellite InSAR dataset acquired in descending (left) and ascending (right) geometries over the study area. The base image is a Sentinel-2 optical image of the mine before the event (10 m pixel resolution).

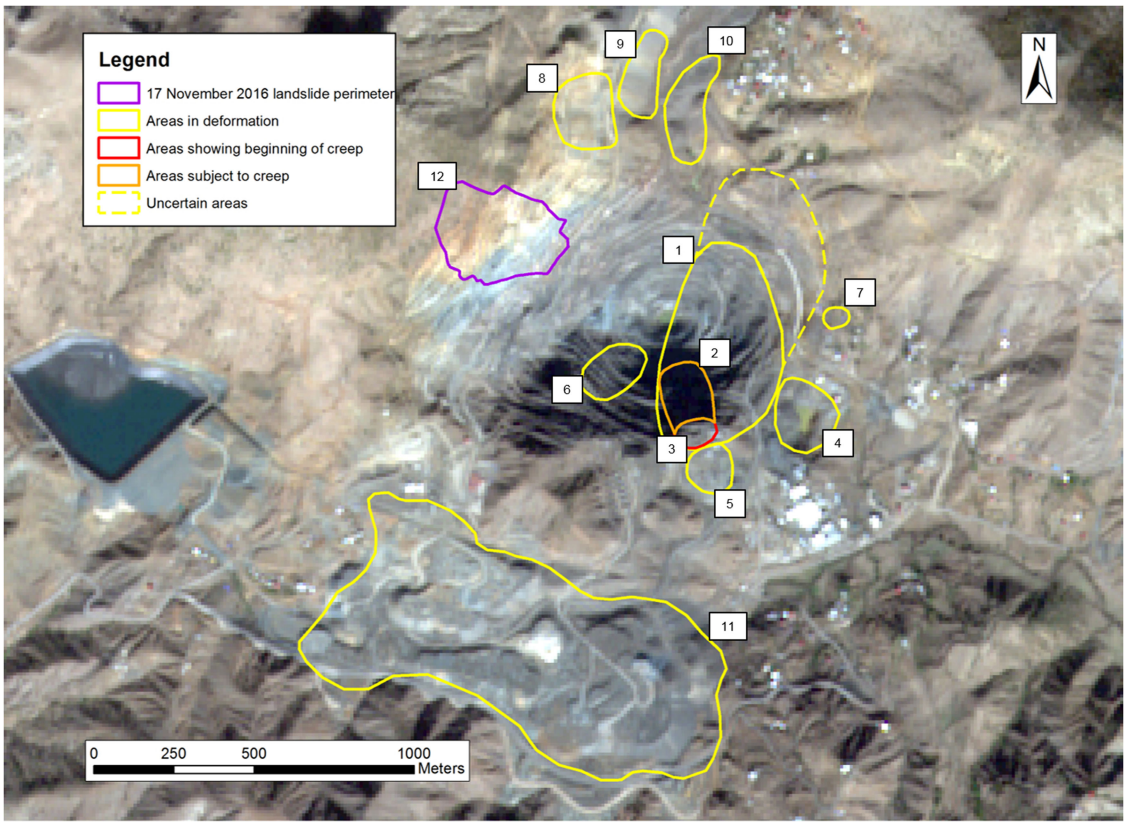

Fig. 4. Delimitation of the primary areas of ground deformation, as defined through the analysis of the InSAR satellite datasets. The base image is a Sentinel-2 optical image of the mine before the event (10 m pixel resolution).

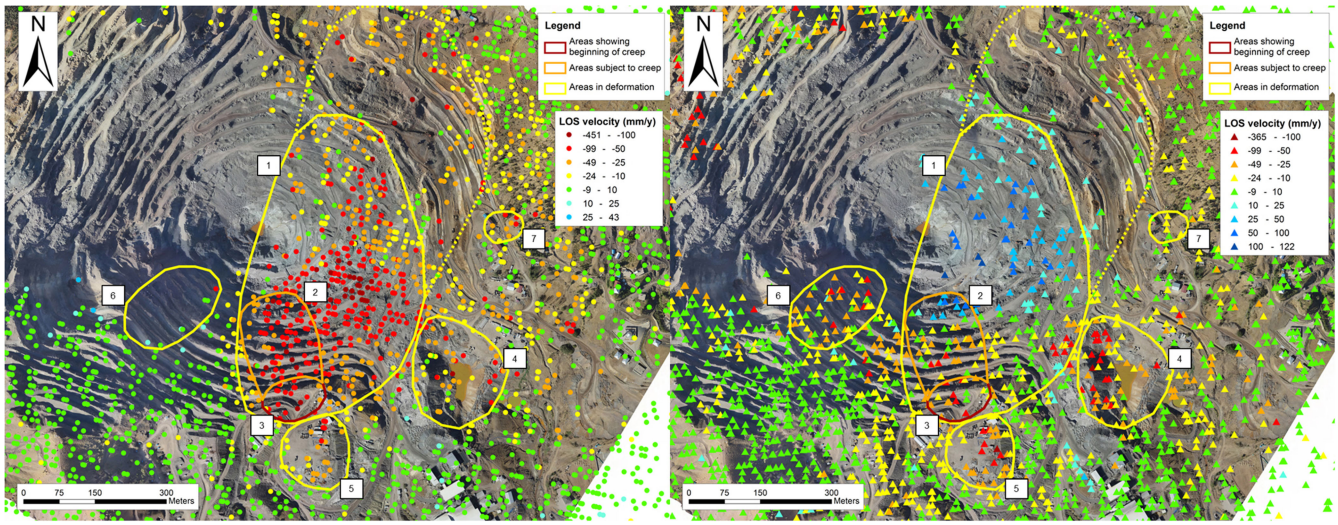

Fig. 5. PS and DS acquired in descending (left) and ascending (right) geometries across areas #1–#7, colored according to their LOS velocity. The yellow dashed line represents areas of uncertain attribution. The base image is obtained from a photogrammetric survey of a fixed wing drone carried out on September 29, 2016.

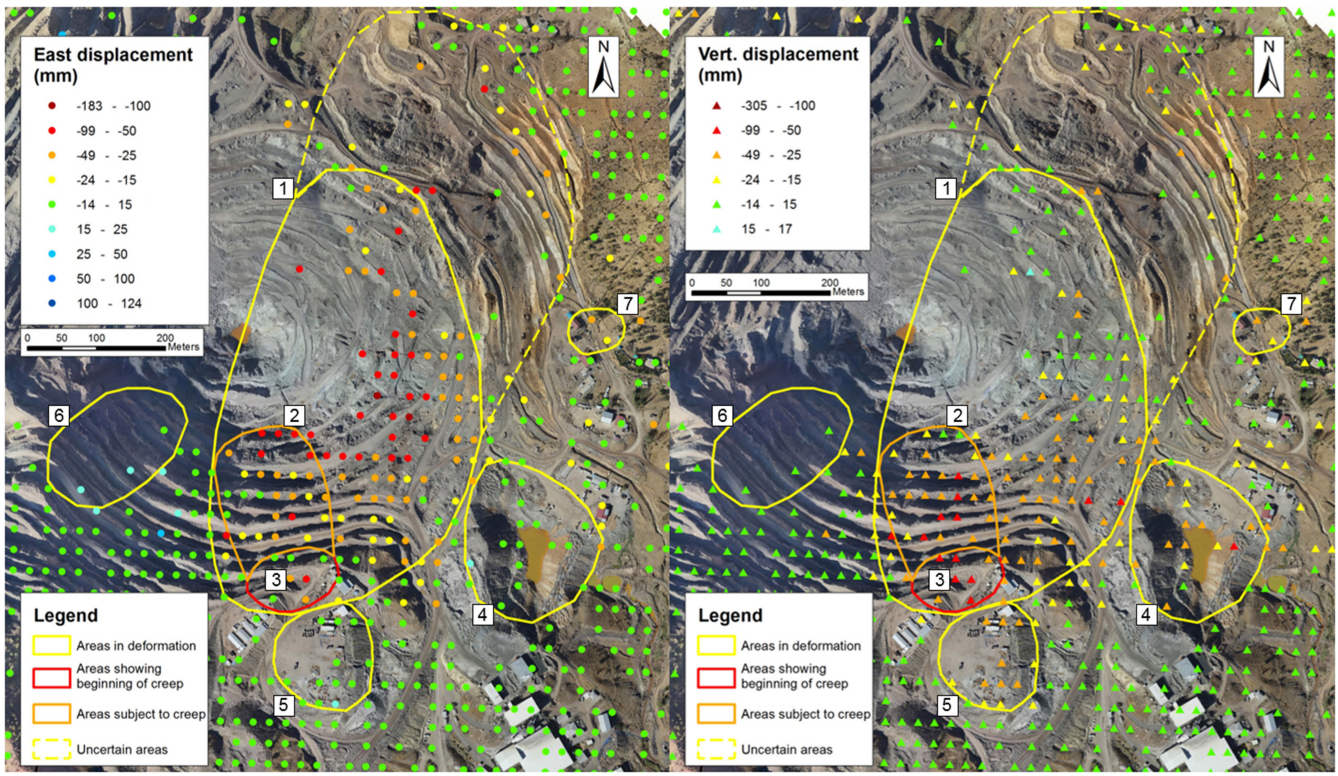

Fig. 6. E–W (left) and vertical (right) displacements obtained from a resampling of ascending and descending InSAR data across areas #1–#7. The base image is obtained from a photogrammetric survey of a fixed wing drone carried out on September 29, 2016.

its inverse will tend toward zero. A more detailed dissertation on landslide forecasting methods at slope scale can be found in [73].

Combining the criteria mentioned above in this section, 12 areas affected by superficial displacements have been identified and interpreted as follows.

Area #1 covers roughly half of the pit and stands out for size and intensity of the measured slope displacements (see Figs. 4–6). The spatial extension of the deforming area suggests that the movement may be complex, and therefore it may be difficult to identify specific structural and geometrical features based only on satellite data. The dashed yellow polygon identifies an area where interpretation of the limits of the deforming pit sector is uncertain; this is caused by a lower density of radar targets, probably owing to ongoing production works.

The red arc (area #3) indicates the only instance where an initial phase of accelerating creep in the displacements of the radar targets is clearly observed, as of November 21, 2016

(see Figs. 5 and 6). The orange polygon immediately downslope (area #2) is instead associated with an area that, for geomorphological reasons, may be subject to the propagation of the accelerating creep from the unstable zone above. Specifically, the radar targets therein might display very early signs of such a trend. Examples of these time series will be shown and discussed in Section IV-B.

Areas #4 and #5 (see Fig. 5) and areas #8–#10 (see Fig. 4) are identified outside of the edge of the pit, in correspondence of accumulations of loose material. In all cases, the trend of deformation is in fact mostly linear, and no significant variation of movement rate is observed during the monitoring period. No significant differences are observed between ascending and descending geometries (see Fig. 3). The topography and the decomposition of the radar measurements in terms of the E–W and vertical directions give clear indication that such deformations are mostly associated with the compaction of the loose material; in fact, vertical movements are much larger than E–W movements, whose magnitude is close to zero (see Fig. 6).

Similarly, area #11, located to the S of the pit (see Figs. 3 and 4), corresponds to a deforming sector, which was used for waste dumping during the monitoring period. The active works in the area determines that the coverage of radar targets on the ground is not complete. In fact, where operations are on-going, the changes in topography do not allow for the identification of radar natural reflectors (one of the conditions for an area on the surface to be classified as a radar reflector is its persistence on all the satellite images used for the multi-interferogram InSAR analysis). Still, a significant number of radar targets could be identified and evidenced intense deformation regardless of the acquisition geometry. In particular, LOS velocities $>$400 mm/y in descending geometry and $>$300 mm/y in ascending geometry were recorded. Since both the acquisition geometries indicate significant movements away from the sensor, it can be inferred that the dominant part of the deformation is due to vertical compaction of the waste material.

Area #6 is a slope sector located in the SW part of the pit ($\sim$25,000 m^2; Fig. 5). In general, the magnitude of the displacements of this area is low and slowly decelerating. Even if only few points can be extracted for the decomposition of the movements, it can be assessed that only those in the E–W direction are significant (see Fig. 6). Such a behavior is consistent with the occurrence of slope relaxation or of slow slope creep and is, therefore, compatible with an instability that currently does not show signs of progressive movements that may be associated with an evolution toward a condition of failure.

Area #7 is a small sector ($\sim$5200 m^2) located in correspondence of a section of a gravel road just outside the eastern edge of the pit (see Fig. 5). The characteristics of the E–W and vertical movements are comparable (see Fig. 6), with descending LOS velocities always $<$100 mm/y. This area is consistent with a slow and shallow translational movement locally affecting the road track. Based on the limited size of the instability, it is inferred that this involves only the superficial soil material, and not the bedrock.

A different case is area #12 (see Figs. 3 and 4), where a failure involving around 414 000 m^3 of material occurred on November 17, 2016. A clear accelerating creep (discussed in the next section) could have been identified roughly three weeks before the collapse. The accelerating creep behavior started in the central part of the landslide and then propagated retrogressively until failure occurred. The boundaries of the landslide before failure could have been reconstructed only with data acquired in ascending geometry, as no coverage of the area was provided with descending geometry, due to the unfavorable aspect and steep slope.

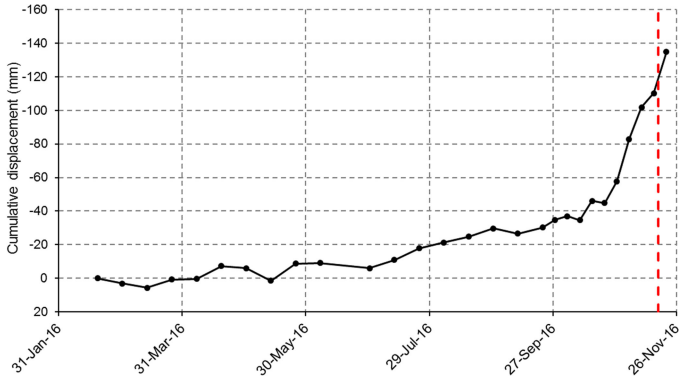

Fig. 7. Displacement time series from February 19 to November 21, 2016 from the radar target displaying the highest deformation within area #12. The red dashed line indicates the time of failure drone carried out on September 29, 2016.

B. Accelerating Time Series

Among the areas that have been identified, some display accelerating time series characterized by different intensities.

The most interesting behavior is observed in the central part of area #12, from where the persistent scatterer with the highest displacement is displayed (see Fig. 7). The initial part of the series depicts a mild linear trend leading to roughly 34.5 mm of displacement from February 19, 2016 to October 10, 2016. Then, data display an accelerating creep that reaches a total displacement of 110.2 mm as of November 15, 2016, the time of the last acquisition before failure.

Calculating the velocity produces a slightly noisy time series, which requires the application of a simple averaging (consisting in a three-measurement moving average) [68], before that the inverse velocity method [36] can be applied (see Figs. 8 and 9).

Fig. 9 depicts the inverse velocity plot, which displays a very good linear fitting toward the x-axis between 28 October and 15 November ($R^2 = 0.81$, black line in Fig. 9), which would suggest a failure around 26 November; on the other hand, the last measurement before failure shows a strong deceleration (possibly related to noise; Fig. 8), which would have made excluding it from the time of failure computation a reasonable decision. Of course, it is easy to determine what data should have been discarded after that the failure has taken place. In any case, if the last measurement was discarded, a more precise forecasting would have been made. According to it, in fact, the time of failure is expected at 7:02 P.M. on 16 November (turquoise line in Fig. 9, with $R^2 = 0.98$), roughly 1 day before the landslide actually occurred, with an estimated precision of $\pm$1 day (while it could have been hourly with a less noisy ground-based instrumentation providing a higher frequency of

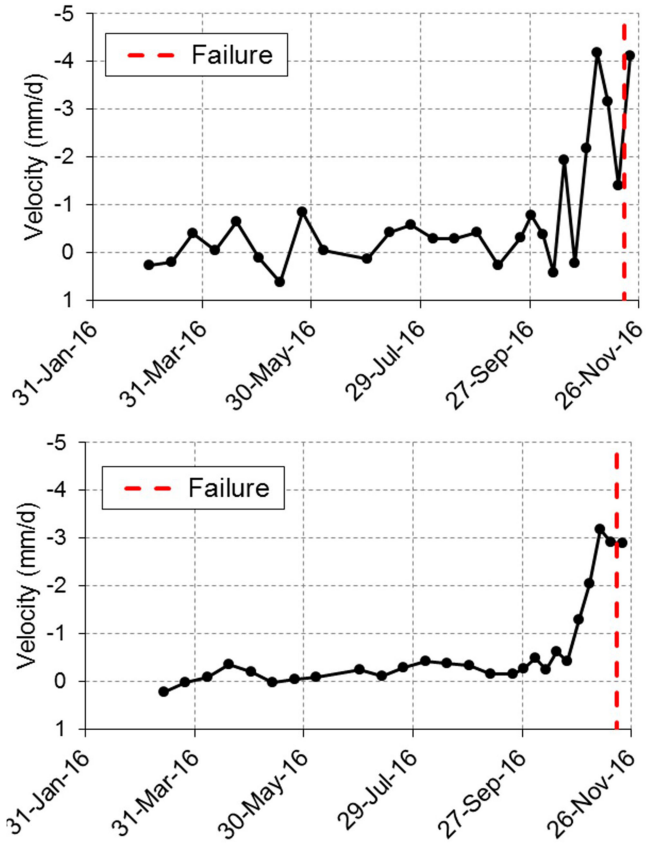

Fig. 8. Average velocity time series of the radar target characterized by the highest amount of total measured deformation within the instability (above) and relative smoothed series (below).

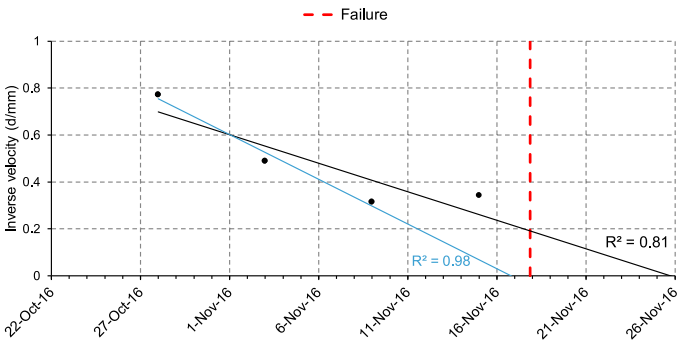

Fig. 9. Linear regressions of the inverse velocity plot derived from the smoothed velocity time series in Fig. 8 (below). The blue line interpolates data from October 22 to November 9, 2016, whereas the black line arrives to November 15, 2016.

acquisition). In both cases (turquoise and black lines) the evident trends provide, with significant advance, a clear indication that a failure process was underway; in fact, this evaluation could have been made as far as approximately 1 week before the event by an experienced user.

Hints of the initiation of an accelerating creep at least since mid-October 2016 (red shaded zone in Fig. 10) are also provided by the displacement time series available for area #2 and, in particular, area #3, which fall within the larger area #1 (see Fig. 5). It can be assumed that area #2 may become subject

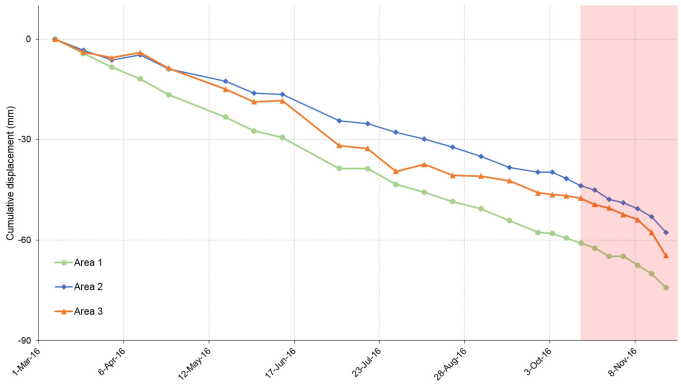

Fig. 10. Average time series of displacement of areas #1–3. The red shaded zone indicates the initiation of the accelerating creep for area #3 and possibly area #2.

to a downslope propagation of the instability of area #3, located above. For comparison, most of area #1 has been deforming at a basically steady rate during the entire period of monitoring (see Fig. 10).

V. Discussions

InSAR has been considered as a useful tool for carry out effective BCM [2]. However, so far, the revisiting time of satellites was hardly sufficient to observe the initiation of accelerating creep and so to provide meaningful warnings.

Nonetheless, this application still presents difficulties in the framework of a near-real time monitoring. In fact, the processing of satellite InSAR data and the update of the relative PS time series are not performed with each new acquisition but require the analysis of a stack of images. As a result, the identification of any accelerating creep behavior can be made only if the latest update of InSAR data happens to be delivered right before the slope failure (few days before at most), although a different schedule might be programmed in case of increased alert.

In any case, even when there are no landslides close to failure and so forecasting methods are not required, the identification of smaller accelerations and linear trends can provide useful insight of the stability condition of the slopes and of the volumes in play. InSAR data acquired every six days (or even daily, in case of Cosmo Sky-Med acquiring in tandem mode) can give precious information concerning the setting of warning thresholds, choices on safety procedures, and on how and where to continue the exploitation of the mine.

This monitoring has relevant applications in the mining industry by highlighting the areas where dedicated in situ geological investigations and integrative monitoring should be implemented (e.g., installation of inclinometric tubes), as well as geological and geomechanical surveys aimed at identifying the potential layer(s) or plane(s) of weakness over which movements may occur.

An interesting use of these data is the reconstruction of the geometry of the sliding surfaces, as described in Section II.

The slope displacements relative to area #1 (see Fig. 5) may be associated with two distinct phenomena, one located in the SSE sector of the pit and the other in the NE sector of the pit (see Fig. 11), with the likely directions of movement being toward

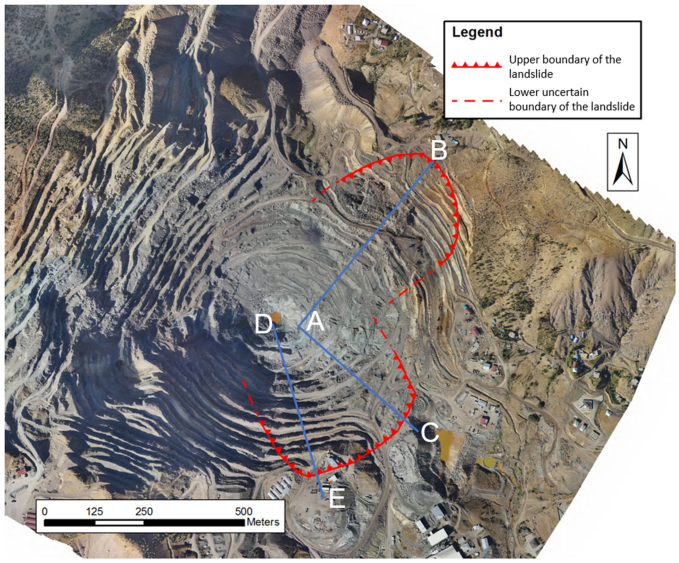

Fig. 11. Interpretation of the deformation field in area #1. The base image is obtained from a photogrammetric survey of a fixed wing drone carried out on September 29, 2016.

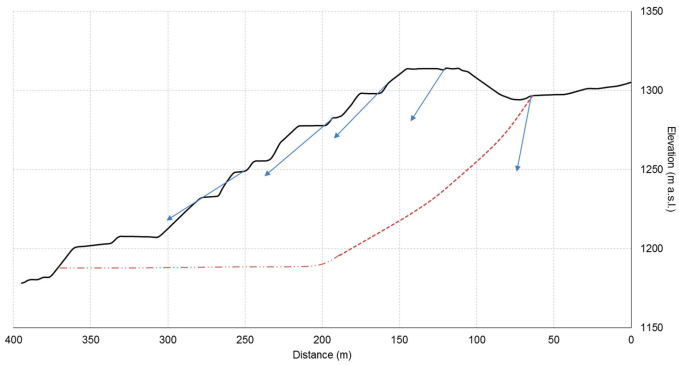

Fig. 12. Interpretation of the sliding surface of the SSE sector of area #1 (the cross section is relative to the AC profile in Fig. 11).

NNW and WSW, respectively. These two slope instabilities may coalesce at the respective toe areas, in proximity of the bottom of the pit.

In order to gain more insight into the geometry of the slope movements, three topographical cross-sections were traced, one for each landslide (see cross-section AC, visible in Figs. 11 and 12, and cross-section AB, visible in Figs. 11 and 13) plus one (named DE) along the zone showing a creep behavior (areas #2 and #3; Figs. 11 and 14). In-SAR data in proximity of the three traces have been analyzed. By using the vertical component of the movement and the E–W component reprojected along the expected direction of actual slope movement (in fact, once the horizontal E-W component is obtained, it was necessary to project it again in case the cross section was not E–W oriented), it was possible to extract movement vectors that could have been plotted on such profiles, allowing for an estimation of the geometry of the hypothetical sliding surfaces (see Figs. 12–14), as described in Section II. The light red part of the sliding surfaces in Figs. 12 and 14 was subjectively extrapolated beyond the last estimated point obtained from the used method.

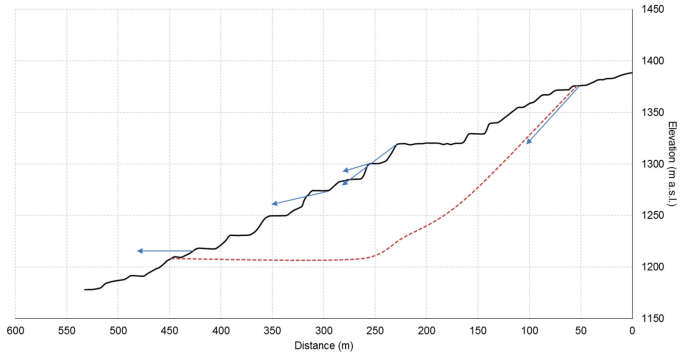

Fig. 13. Interpretation of the sliding surface of the NE sector of area #1 (the cross section is relative to the AB profile in Fig. 11).

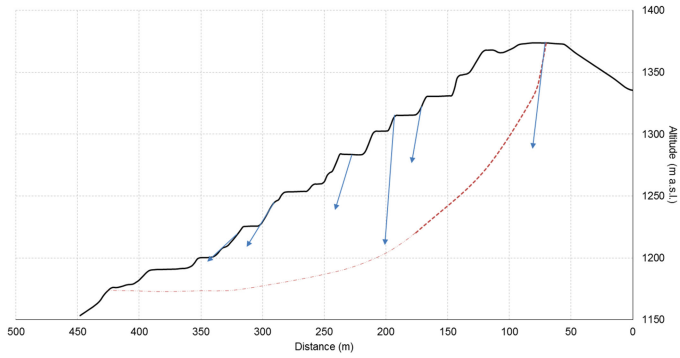

Fig. 14. Interpretation of the sliding surface in correspondence of area #2 and area #3 (the cross section is relative to DE profile in Fig. 11).

It should be noted that the abovementioned method is a simplified method that assumes the movement of single rigid blocks between two consecutive displacement vectors along the analyzed profile, with no internal deformation; therefore, it cannot be used to define local or specific geometrical features of the landslides. Still, crucial information regarding the expected failure mode and depth of the detected moving area may be extrapolated.

Cross-section DE has been traced to verify if the accelerating creep movement detected could have been attributed to a shallower phenomenon falling within the larger unstable area. By comparing the reconstructed sliding surfaces along cross-section AC (see Fig. 12) and DE (see Fig. 14), they appear similar and consistent with a unique, deep sliding surface interesting the whole SSE sector of the pit.

The results of the analysis evidenced a general roto-translational mechanism of movement, with an estimated average depth of the sliding surface of approximately 30–40 m; the same geometry and depth can be evinced from the AB cross-section (see Fig. 13). This would yield volumes of approximately 3.2×106 m^3 and 2.7×106 m^3 for the SSE and NE landslide, respectively.

With the exception of the subsectors identified as area #2 and area #3, the general trend of deformation is mostly linear and, thus, suggesting that these landslides are not expected to fail in the near future.

VI. Conclusion

The launch of Sentinel satellites opened new possibilities to ground movement monitoring and early warning that with previous satellites were only object of simulations. This constellation is able to exploit a six-days revisiting time, thus enabling the study of slopes over regional areas with a frequency previously not reachable. This brings a major change especially as far as early warning activities are concerned.

In this article, we have shown a real case study from an open-pit copper mine that illustrates how an appropriate use of Sentinel data can be employed to identify, map, and characterize in kinematic terms subsiding areas and landslides, prospectively forecasting failures. The high density of measurement points also allowed for the estimation of the sliding surface shape and depth, obtained through geometrical arguments. Following the creep theory, displacement time series have been clustered according to their kinematic behavior, stressing the importance of those regions where accelerating trend were taking place. A timely and informed usage of these data would have likely led to a correct prediction of a large slope failure that occurred in the mine.

Other than giving the possibility to perform predictions, this tool, also thanks to the free availability of the datasets and to the relatively high spatial density of reflectors, can provide other important planning applications in open-pit mines management, and can be useful for programming interventions, deciding if and where to relocate the extracting activities, designing safe routes for the operators, and setting trigger action response plans.

Here, we have wanted to show how Sentinel-1 used for open-pit mines can be regarded as a tool to formulate hypotheses that are strongly based on reliable data; however, the intrinsic limitations of satellite In-SAR still persist (LOS measurements, discontinuous spatial coverage, possibility of noise, phase wrapping); with respect to ground-based interferometric radar, commonly used to monitor landslides and quarries [7], [74]–[76], the lower frequency of acquisition of satellites allows for meaningful early warnings only for those landslides displaying a slower evolution (which are typically not small sized and not occurring in stiff rocks; [10], [70], [73]). Therefore, the high potential of Sentinel-1 in this matter should not dismiss the importance of field surveys and integrated monitoring to complete and verify such hypotheses.

References

[1] E. Intrieri, G. Gigli, N. Casagli, and F. Nadim, "Brief communication: Landslide early warning system: Toolbox and general concepts," *Natural Hazards Earth Syst. Sci.*, vol. 13, pp. 85–90, 2013.

[2] J. Read and P. Stacey, *Guidelines for Open Pit Slope Design*. Melbourne, Vic, Australia: CSIRO Publ., 2009.

[3] D. D. Kim, R. B. Langley, J. Bond, and A. Chrzanowski, "Local deformation monitoring using GPS in an open pit mine: Initial study," *GPS Solution*, vol. 7, no. 3, pp. 176–185, 2003.

[4] N. Brown, S. Kaloustian, and M. Roeckle, "Monitoring of open pit mines using combined GNSS satellite receivers and robotic total stations," in *Proc. Int. Symp. Rock Slope Stability Open Pit Mining Civil Eng. Australian Centre Geomech.*, 2007, pp. 417–429.

[5] S. Calvari, E. Intrieri, F. Di Traglia, A. Bonaccorso, N. Casagli, and A. Cristaldi, "Monitoring crater-wall collapse at active volcanoes: A study of the 12 January 2013 event at Stromboli," *Bull. Volcanol.*, vol. 78, no. 39, pp. 1–16, 2016.

[6] M. Barla, F. Antolini, D. Bertolo, P. Thuegaz, D. D'Aria, and G. Amoroso, "Remote monitoring of the Comba Citrin landslide using discontinuous GBInSAR campaigns," *Eng. Geol.*, vol. 222, pp. 111–123, 2017.

[7] O. Monserrat, M. Crosetto, and G. Luzi, "A review of ground-based SAR interferometry for deformation measurement," *ISPRS J. Photogram. Remote Sens.*, vol. 93, pp. 40–48, 2014.

[8] D. Tarchi *et al.*, "Landslide monitoring by using ground-based SAR interferometry: An example of application to the Tessina landslide in Italy," *Eng. Geol.*, vol. 68, no. 1/2, pp. 15–30, 2003.

[9] N. Harries, D. Noon, and K. Rowley, "Case studies of slope stability radar used in open cut mines," in *Stability of Rock Slopes in Open Pit Mining and Civil Engineering Situations*. Johannesburg, South Africa: SAIMM, 2006, pp. 335–342.

[10] T. Carlà, P. Farina, E. Intrieri, K. Botsialas, and N. Casagli, "On the monitoring and early-warning of brittle slope failures in hard rock masses: Examples from an open-pit mine," *Eng. Geol.*, vol. 228, pp. 71–81, 2017.

[11] C. Carnec, D. Massonnet, and C. King, "Two examples of the use of SAR interferometry on displacement fields of small spatial extent," *Geophy. Res. Lett.*, vol. 23, no. 24, pp. 3579–3852, 1996.

[12] P. Canuti, N. Casagli, L. Ermini, R. Fanti, and P. Farina, "Landslide activity as a geoindicator in Italy: Significance and new perspectives from remote sensing," *Environ. Geol.*, vol. 45, no. 7, pp. 907–919, 2004.

[13] P. Farina, D. Colombo, A. Fumagalli, F. Marks, and S. Moretti, "Permanent scatterers for landslide investigations: Outcomes from the ESA-SLAM project," *Eng. Geol.*, vol. 88, no. 3, pp. 200–217, 2006.

[14] J. C. García-Davalillo, G. Herrera, D. Notti, and T. Strozzi, "DInSAR analysis of ALOS PALSAR images for the assessment of very slow landslides: The Tena valley case study," *Landslides*, vol. 11, no. 2, pp. 225–246, 2013.

[15] F. Bardi *et al.*, "Integration between ground based and satellite SAR data in landslide mapping: The San Fratello case study," *Geomorphology*, vol. 223, pp. 45–60, 2014.

[16] F. Bardi *et al.*, "Space-borne and ground-based InSAR data integration: The Åknes test site," *Remote Sens.*, vol. 8, no. 3, 2016, Art. no. 237.

[17] L. Solari *et al.*, "Fast detection of ground motions on vulnerable elements using Sentinel-1 InSAR data," *Geomatics, Natural Hazards Risk*, vol. 9, no. 1, pp. 152–174, 2018.

[18] D. Massonnet *et al.*, "The displacement field of the Landers earthquake mapped by radar interferometry," *Nature*, vol. 364, pp. 138–142, 1993.

[19] G. Peltzer and P. Rosen, "Surface displacement of the 17 May 1993 Eureka Valley, California, earthquake observed by SAR interferometry," *Science*, vol. 268, pp. 1333–1336, 1995.

[20] D. Massonnet, P. Briole, and A. Arnaud, "Deflation of Mount Etna monitored by spaceborne radar interferometry," *Nature*, vol. 375, pp. 567–570, 1995.

[21] D. Massonnet and F. Sigmundsson, "Remote sensing of volcano deformation by radar interferometry from various satellites," in *Remote Sensing of Active Volcanism*, P. J. Mouginis-Mark, J. A. Crisp, and J. H. Fink, Eds. Washington, DC, USA: Amer. Geophys. Union, 2000.

[22] B. Antonielli *et al.*, "Pre-eruptive ground deformation of Azerbaijan mud volcanoes detected through satellite radar interferometry (DInSAR)," *Tectonophysics*, vol. 637, pp. 163–177, 2014.

[23] D. L. Galloway *et al.*, "Detection of aquifer system compaction and land subsidence using interferometric synthetic aperture radar, Antelope Valley, Mojave Desert, California," *Water Resour. Res.*, vol. 34, no. 10, pp. 2573–2585, 1998.

[24] F. Amelung, D. L. Galloway, J. W. Bell, and H. Zebker, "Sensing the ups and downs of Las Vegas: InSAR reveals structural control of land subsidence and aquifer-system deformation," *Geology*, vol. 27, no. 6, pp. 483–486, 1999.

[25] A. Ferretti, C. Prati, and F. Rocca, "Non linear subsidence rate estimation using permanent scatterers in differential SAR interferometry," *IEEE Trans. Geosci. Remote Sens.*, vol. 38, no. 5, pp. 2202–2212, Sep. 2000.

[26] D. Colombo, P. Farina, S. Moretti, G. Nico, and C. Prati, "Land subsidence in the Firenze–Prato–Pistoia basin measured by means of spaceborne SAR interferometry," in *Proc. IEEE Int. Geosci. Remote Sens. Symp.*, Tolouse, France, Jul. 21–25, 2003, pp. 2927–2929.

[27] P. Farina, P. Canuti, N. Casagli, A. Ferretti, F. Marks, and G. Menduni, "Survey and geological characterisation of land subsidence phenomena in the Lucca plain (Italy) using PSInSAR," *Geophys. Res. Abstr.*, vol. 8, 2006, Art. no. 07930.

[28] L. W. Kenyi and V. Kaufmann, "Estimation of rock glacier surface deformation using SAR interferometry data," *IEEE Trans. Geosci. Remote Sens.*, vol. 41, no. 6, pp. 1512–1515, Jun. 2003.

[29] T. Strozzi *et al.*, "Survey and monitoring of landslide displacements by means of L-band satellite SAR interferometry," *Landslides*, vol. 2, no. 3, pp. 193–201, 2005.

[30] F. Catani, N. Casagli, L. Ermini, G. Righini, and G. Menduni, "Landslide hazard and risk mapping at catchment scale in the Arno River basin," *Landslides*, vol. 2, pp. 329–342, 2005.

[31] J. Wasowski and F. Bovenga, "Investigating landslides and unstable slopes with satellite multi temporal interferometry: Current issues and future perspectives," *Eng. Geol.*, vol. 174, pp. 103–138, 2014.

[32] M. Crosetto, O. Monserrat, M. Cuevas-Gonzalez, N. Devanthery, and B. Crippa, "Persistent scatterer interferometry: A review," *ISPRS J. Photogramm.*, vol. 115, pp. 78–89, 2016.

[33] A. Barra, O. Monserrat, P. Mazzanti, C. Esposito, M. Crosetto, and G. Scarascia Mugnozza, "Potentiality of SENTINEL-1 for landslide detection: First results in the Molise Region (Italy)," in *Proc. Eur. Geosci. Union General Assembly Conf.*, 2016, vol. 18, p. 2916.

[34] A. Novellino, F. Cigna, M. Brahmi, A. Sowter, L. Bateson, and S. Marsh, "Assessing the feasibility of a national InSAR ground deformation map of Great Britain with Sentinel-1," *Geosciences*, vol. 7, no. 2, pp. 1–14, 2017.

[35] F. Raspini *et al.*, "Continuous, semi-automatic monitoring of ground deformation using Sentinel-1 satellites," *Sci. Rep.*, vol. 8, 2018, Art. no. 7253.

[36] T. Fukuzono, "A method to predict the time of slope failure caused by rainfall using the inverse number of velocity of surface displacement," *J. Japanese Landslide Soc.*, vol. 22, pp. 8–13, 1985.

[37] T. Carlà, P. Farina, E. Intrieri, H. Ketizmen, and N. Casagli, "Integration of ground-based radar and satellite InSAR data for the analysis of an unexpected slope failure in an open-pit mine," *Eng. Geol.*, vol. 235, pp. 39–52, 2018.

[38] E. Intrieri *et al.*, "The Maoxian landslide as seen from space: Detecting precursors of failure with Sentinel-1 data," *Landslides*, vol. 15, no. 1, pp. 123–133, 2018.

[39] E. Intrieri, T. Carlà, and G. Gigli, "Forecasting the time of failure of landslides at slope-scale: A literature review," *Earth-Sci. Rev.*, vol. 193, pp. 333–349, 2019 (in French).

[40] N. Casagli *et al.*, "Spaceborne, UAV and ground-based remote sensing techniques for landslide mapping, monitoring and early warning," *Geoenviron. Disasters*, vol. 4, no. 9, pp. 1–23, 2017.

[41] H. A. Zebker and R. M. Goldstein, "Topographic mapping from interferometric synthetic aperture radar observations," *J. Geophys. Res., Solid Earth*, vol. 91, no. B5, pp. 4993–4999, 1986.

[42] A. K. Gabriel, R. M. Goldstein, and H. A. Zebker, "Mapping small elevation changes over large areas: Differential radar interferometry," *J. Geophys. Res., Solid Earth*, vol. 94, no. B7, pp. 9183–9191, 1989.

[43] D. Massonnet and T. Rabaute, "Radar interferometry: Limits and potential," *IEEE Trans. Geosci. Remote Sens.*, vol. 31, no. 2, pp. 455–464, Mar. 1993.

[44] R. M. Goldstein, H. A. Zebker, and C. L. Werner, "Satellite radar interferometry: Two-dimensional phase unwrapping," *Radio Sci.*, vol. 23, no. 4, pp. 713–720, 1988.

[45] D. Massonnet and K. L. Feigl, "Radar interferometry and its application to changes in the Earth's surface," *Rev. Geophys.*, vol. 36, no. 4, pp. 441–500, 1998.

[46] D. Tarchi *et al.*, "Landslide monitoring by using ground-based SAR interferometry: An example of application to the Tessina landslide in Italy," *Eng. Geol.*, vol. 68, no. 1/2, pp. 15–30, 2003.

[47] G. Luzi *et al.*, "Ground-based radar interferometry for landslides monitoring: Atmospheric and instrumental decorrelation sources on experimental data," *IEEE Trans. Geosci. Remote Sens.*, vol. 42, no. 11, pp. 2454–2466, Nov. 2004.

[48] C. Colesanti, A. Ferretti, C. Prati, and F. Rocca, "Monitoring landslides and tectonic motion with the permanent scatterers technique," *Eng. Geol.*, vol. 68, pp. 3–14, 2003.

[49] A. Ferretti, C. Prati, and F. Rocca, "Permanent scatterers in SAR interferometry," *IEEE Trans. Geosci. Remote Sens.*, vol. 39, no. 1, pp. 8–20, Jan. 2001.

[50] C. Meisina *et al.*, "The use of PSInSAR and SqueeSAR techniques for updating landslide inventories," in *Landslide Science and Practice*. Berlin, Germany: Springer, 2013, pp. 81–87.

[51] E. Lagios *et al.*, "SqueeSAR and GPS ground deformation monitoring of Santorini Volcano (1992–2012): Tectonic implications," *Tectonophysics*, vol. 594, pp. 38–59, 2013.

[52] A. Tamburini, S. Del Conte, G. Larini, L. Lopardo, C. Malaguti, and P. Vescovi, "Application of SqueeSAR to the characterization of deep seated gravitational slope deformations: The Berceto case study (Parma, Italy)," in *Landslide Science and Practice*. Berlin, Germany: Springer, 2013, pp. 437–443.

[53] M. Carter and S. P. Bentley, "The geometry of slip surfaces beneath landslides: Predictions from surface measurements," *Can. Geotech. J.*, vol. 22, pp. 234–238, 1985.

[54] D. Cruden, "The geometry of slip surfaces beneath landslides: Predictions from surface measurements: Discussion," *Can. Geotech. J.*, vol. 23, no. 1, p. 94, 1986.

[55] A. Ferretti *et al.*, "Submillimeter accuracy of InSAR time series: Experimental validation," *IEEE Trans. Geosci. Remote Sens.*, vol. 45, no. 5, pp. 1142–1153, May 2007.

[56] A. H.-M. Ng, L. Ge, K. Zhang, and X. Li, "Monitoring ground deformation in Beijing, China with persistent scatterer SAR interferometry," *J. Geodesy*, vol. 86, pp. 375–392, 2012.

[57] M. Béjar-Pizarro *et al.*, "Mapping vulnerable urban areas affected by slow-moving landslides using Sentinel-1 InSAR data," *Remote Sens.*, vol. 9, no. 9, 2017, Art. no. 876.

[58] V. Tofani, F. Raspini, F. Catani, and N. Casagli, "Persistent scatterer interferometry (PSI) technique for landslide characterization and monitoring," *Remote Sens.*, vol. 5, no. 3, pp. 1045–1065, 2013.

[59] A. Ferretti, A. Fumagalli, F. Novali, C. Prati, F. Rocca, and A. Rucci, "A new algorithm for processing interferometric data-stacks: SqueeSAR," *IEEE Trans. Geosci. Remote Sens.*, vol. 49, no. 9, pp. 3460–3470, Sep. 2011.

[60] X. L. Ding, G. X. Liu, Z. W. Li, Z. L. Li, and Y. Q. Chen, "Ground subsidence monitoring in Hong Kong with satellite SAR interferometry," *Photogramm. Eng. Remote Sens.*, vol. 70, no. 10, pp. 1151–1156, 2004.

[61] V. Singhroy, "Satellite remote sensing applications for landslide detection and monitoring," in *Landslides–Disaster Risk Reduction*. Berlin, Germany: Springer, 2009, pp. 143–158.

[62] T. Carlà, F. Raspini, E. Intrieri, and N. Casagli, "A simple method to help determine landslide susceptibility from spaceborne InSAR data: The Montescaglioso case study," *Environ. Earth Sci.*, vol. 75, no. 1492, pp. 1–12, 2016.

[63] M. B. Dusseault and C. J. Fordham, "Time-dependent behavior of rocks," in *Comprehensive Rock Engineering*, J. A. Hudson, Ed. Oxford, U.K.: Pergamon Press, 1994, ch. 6, vol. 4, pp. 119–149.

[64] M. Saito, "Forecasting time of slope failure by tertiary creep," in *Proceedings of 7th International Conference on Soil Mechanics and Foundations Engineering*. Oxford, U.K.: Pergamon Press, 1969, pp. 667–683.

[65] C. Azimi, J. Biarez, P. Desvarreux, and F. Keime, "Prévision d'éboulement en terrain gypseux," in *Proc. 5th Int. Symp. Landslides*. Lausanne, Switzerland, 1988, pp. 531–536 (in French).

[66] A. Mufundirwa, Y. Fujii, and J. Kodama, "A new practical method for prediction of geomechanical failure-time," *Int. J. Rock Mech. Mining*, vol. 47, no. 7, pp. 1079–1090, 2010.

[67] G. B. Crosta and F. Agliardi, "Failure forecast for large rock slides by surface displacement measurements," *Can. Geotech. J.*, vol. 40, pp. 176–191, 2003.

[68] T. Carlà, E. Intrieri, F. Di Traglia, T. Nolesini, G. Gigli, and N. Casagli, "Guidelines on the use of inverse velocity method as a tool for setting alarm thresholds and forecasting landslides and structure collapses," *Landslides*, vol. 14, no. 2, pp. 517–534, 2016.

[69] G. J. Dick, E. Eberhardt, A. G. Cabrejo-Liévano, D. Stead, and N. D. Rose, "Development of an early-warning time-of-failure analysis methodology for open-pit mine slopes utilizing ground-based slope stability radar monitoring data," *Can. Geotech. J.*, vol. 52, pp. 515–519, 2015.

[70] E. Intrieri and G. Gigli, "Landslide forecasting and factors influencing predictability," *Natural Hazards Earth Syst. Sci.*, vol. 16, pp. 2501–2510, 2016.

[71] D. N. Petley, D. J. Petley, and R. J. Allison, "Temporal prediction in landslides—Understanding the Saito effect," in *Proc. of 10th Int. Symp. Landslides Eng. Slopes*, Xi'an, China, 2008, pp. 865–871.

[72] N. D. Rose and O. Hungr, "Forecasting potential rock slope failure in open pit mines using the inverse velocity method," *Int. J. Rock Mech. Mining Sci.*, vol. 44, pp. 308–320, 2007.

[73] E. Intrieri, T. Carlà, and G. Gigli, "Forecasting the time of failure of landslides at slope-scale: a literature review," *Earth-Sci. Rev.*, vol. 193, pp. 333–349, 2019.

[74] M. Crosetto, O. Monserrat, G. Luzi, M. Cuevas, and N. Devanthéry, "Deformation monitoring using ground-based SAR data," in *Engineering Geology for Society and Territory*. Cham, Switzerland: Springer, 2015, vol. 5, pp. 137–140.

[75] L. Lombardi *et al.*, "The Calatabiano landslide (southern Italy): Preliminary GB-InSAR monitoring data and remote 3D mapping," *Landslides*, vol. 14, no. 2, pp. 685–696, 2017.

[76] F. Antolini, M. Barla, G. Gigli, A. Giorgetti, E. Intrieri, and N. Casagli, "Combined finite-discrete numerical modeling of runout of the Torgiovannetto di Assisi rockslide in central Italy," *Int. J. Geomech.*, vol. 16, no. 6, 2016, Art. no. 04016019.